AMERICAN SOCIETY FOR MICROBIOLOGY | mBio®

RESEARCH ARTICLE

Extracellular Electron Transfer Powers *Enterococcus faecalis* Biofilm Metabolism

Damien Keogh,[a] Ling Ning Lam,[a,b] Lucinda E. Doyle,[a,c] Artur Matysik,[a] Shruti Pavagadhi,[d] Shivshankar Umashankar,[d] Pui Man Low,[a] Jennifer L. Dale,[e] Yiyang Song,[f] Sean Pin Ng,[f] Chris B. Boothroyd,[g] Gary M. Dunny,[e] Sanjay Swarup,[d,h] Rohan B. H. Williams,[d] Enrico Marsili,[a,i] Kimberly A. Kline[a,b]

[a]Singapore Centre for Environmental Life Science Engineering, Nanyang Technological University, Singapore
[b]School of Biological Sciences, Nanyang Technological University, Singapore
[c]Interdisciplinary Graduate School, Nanyang Technological University, Singapore
[d]Singapore Centre for Environmental Life Science Engineering, National University of Singapore, Singapore
[e]Department of Microbiology, University of Minnesota Medical School, Minneapolis, Minnesota, USA
[f]Singapore Phenome Center, Lee Kong Chian School of Medicine, Nanyang Technological University, Singapore
[g]School of Materials Science and Engineering, Nanyang Technological University, Singapore
[h]Department of Biological Sciences, National University of Singapore, Singapore
[i]School of Chemical and Biomedical Engineering, Nanyang Technological University, Singapore

ABSTRACT Enterococci are important human commensals and significant opportunistic pathogens. Biofilm-related enterococcal infections, such as endocarditis, urinary tract infections, wound and surgical site infections, and medical device-associated infections, often become chronic upon the formation of biofilm. The biofilm matrix establishes properties that distinguish this state from free-living bacterial cells and increase tolerance to antimicrobial interventions. The metabolic versatility of the enterococci is reflected in the diversity and complexity of environments and communities in which they thrive. Understanding metabolic factors governing colonization and persistence in different host niches can reveal factors influencing the transition to biofilm pathogenicity. Here, we report a form of iron-dependent metabolism for *Enterococcus faecalis* where, in the absence of heme, extracellular electron transfer (EET) and increased ATP production augment biofilm growth. We observe alterations in biofilm matrix depth and composition during iron-augmented biofilm growth. We show that the *ldh* gene encoding L-lactate dehydrogenase is required for iron-augmented energy production and biofilm formation and promotes EET.

IMPORTANCE Bacterial metabolic versatility can often influence the outcome of host-pathogen interactions, yet causes of metabolic shifts are difficult to resolve. The bacterial biofilm matrix provides the structural and functional support that distinguishes this state from free-living bacterial cells. Here, we show that the biofilm matrix can immobilize iron, providing access to this growth-promoting resource which is otherwise inaccessible in the planktonic state. Our data show that in the absence of heme, *Enterococcus faecalis* L-lactate dehydrogenase promotes EET and uses matrix-associated iron to carry out EET. Therefore, the presence of iron within the biofilm matrix leads to enhanced biofilm growth.

KEYWORDS *Enterococcus faecalis*, biofilm, extracellular electron transfer, iron, metabolism

Human colonization by enterococci initiates immediately at birth via gastrointestinal inoculation from maternal sources, diet, and the environment (1). *Enterococcus faecalis* represents a significant proportion of this early enterococcal population and

Received 25 April 2017 **Accepted** 14 March 2018 **Published** 10 April 2018

Citation Keogh D, Lam LN, Doyle LE, Matysik A, Pavagadhi S, Umashankar S, Low PM, Dale JL, Song Y, Ng SP, Boothroyd CB, Dunny GM, Swarup S, Williams RBH, Marsili E, Kline KA. 2018. Extracellular electron transfer powers *Enterococcus faecalis* biofilm metabolism. mBio 9:e00626-17. https://doi.org/10.1128/mBio.00626-17.

Invited Editor Lynn E. Hancock, University of Kansas

Editor Scott J. Hultgren, Washington University School of Medicine

Copyright © 2018 Keogh et al. This is an open-access article distributed under the terms of the Creative Commons Attribution 4.0 International license.

Address correspondence to Kimberly A. Kline, kkline@ntu.edu.sg.

D.K. and L.N.L. contributed equally to this work.

Downloaded from mbio.asm.org on May 14, 2018 - Published by mbio.asm.org

Downloaded from mbio.asm.org on May 14, 2018 - Published by mbio.asm.org

remains a stable member of the community throughout life (1). In the gastrointestinal tract, enterococci are present in the lumen as well as in more specialized niches in the physicochemically complex mucus epithelial layer and epithelial crypts in the small intestine (2).

Bacterial biofilms contribute to host health and disease and are complex systems that rely on the biofilm matrix to provide the structural and functional properties that distinguish this state from free-living bacterial cells (3). The dynamics of biofilm formation are dependent on many factors such as nutrient availability, environmental stress, social competition, and the generation of extracellular matrix materials. These extracellular polymeric substances provide the architecture surrounding the bacterial cells enabling emergent properties such as resource capture, tolerance to antimicrobial compounds, cooperation or competition, and localized gradients. Biofilm-associated enterococcal infections can be especially difficult to treat due to their increased tolerance to antimicrobials and immune clearance (4).

The lactic acid bacteria (LAB), which include enterococci, use an electron transport chain for aerobic respiration when external heme is provided or, alternatively, can perform fermentation in the absence of heme. *E. faecalis* does not synthesize heme *de novo*, and therefore, the bacterium lacks porphyrin rings of heme required for cytochrome *bd* activity during cellular respiration (5). Similar to other members of the lactic acid bacterial group, *E. faecalis* has little or no requirement for nutritional iron, with manganese instead being used as the essential cofactor for cellular processes (6–9). Yet, *E. faecalis* undergoes transcriptional reprogramming when environmental iron availability changes (10–12), suggesting an alternative function of iron for this organism. *E. faecalis* is also remarkably resistant to oxidative stress from O_2^-, hydroxyl radicals ($OH^{\cdot}$), and hydrogen peroxide (H_2O_2) sources from incomplete reduction of oxygen during respiration, from the oxidative action of host immune cells, or that arise during the Fenton reaction (13, 14). These findings suggest that *E. faecalis* may be able to withstand iron at concentrations which are typically toxic to most bacterial species. In human serum, free iron is far below the 10^{-7} to 10^{-5} M optimal range required to support the growth of most bacteria (15). However, iron availability in the host can vary. Disease states such as hemochromatosis and thalassemia disrupt homeostasis and cause excess iron accumulation (16–19). While there are no strong clinical links between iron overload disorders and enterococcal infection in humans, enterococcal overgrowth has been documented in the gastrointestinal tract of mice carrying mutations associated with hereditary hemochromatosis (19), suggesting that there may be physiological niches where enterococci may encounter excess iron. Moreover, iron oxides have also been detected in human spleens and the iron concentration of the gastrointestinal tract is sufficient to support bacterial growth (20, 21).

In this study, we hypothesize that the ability to withstand higher iron concentrations in some environments provides a metabolic advantage to *E. faecalis*. We show that iron can accumulate in the *E. faecalis* biofilm matrix and augments biofilm growth. Using chronocoulometry, we show that iron-augmented biofilms undergo extracellular electron transport (EET), in an *ldh*-dependent manner. Together, these data support a model in which the *E. faecalis* biofilm matrix harbors iron sinks which in turn promote EET, altered metabolism, and augmented biofilm growth. Understanding the metabolic factors that promote colonization and biofilm formation under different environmental conditions may inform mechanisms governing the switch from free-living planktonic to biofilm enterococci in a number of ecologic reservoirs.

RESULTS

Iron supplementation promotes *Enterococcus faecalis* biofilm growth and alters biofilm matrix and matrix properties. To understand the influence of iron on *E. faecalis* biofilm, we evaluated biofilm growth using ferric chloride ($FeCl_3$)-enriched medium. We analyzed biofilm by confocal laser scanning microscopy (CLSM) in the absence (normal) and presence (supplemented) of additional $FeCl_3$ in a flow cell biofilm system. Using a green fluorescent protein (GFP)-expressing *E. faecalis* strain grown in

Downloaded from mbio.asm.org on May 14, 2018 - Published by mbio.asm.org

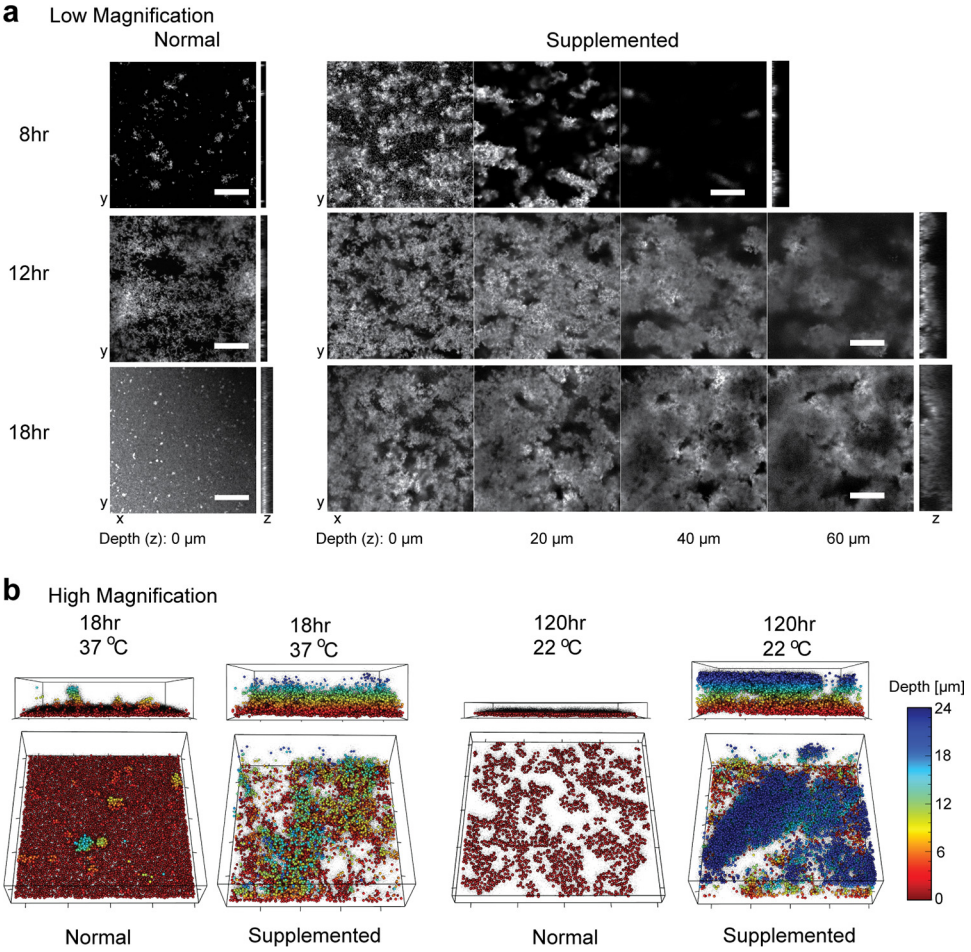

FIG 1 *E. faecalis* flow cell biofilms in iron-supplemented medium. (a) CLSM images at 8, 12, and 18 h for normal (10% TSBG) and supplemented (10% TSBG plus 0.2 mM $FeCl_3$) media. Selected optical sections at the indicated depths are followed by representative lateral views in *yz* at the right of each image set. Bar, 100 μm. (b) 3D reconstructions of high-magnification CLSM stacks of *E. faecalis* flow cell biofilms grown in normal or supplemented medium for 18 h at 37°C or 120 h at 22°C. Biofilm depth is color coded as indicated on *z*-depth scale (0 to 24 μm), and the lateral box dimensions are 85 by 85 μm (20 μm between ticks).

flow cells, we observed augmented biofilm as early as 8 h in medium supplemented with 0.2 mM $FeCl_3$ compared to normal medium (Fig. 1a). Iron-enhanced biofilm growth continued for 18 h, in contrast to the thinner normal biofilm. Iron supplementation did not augment *E. faecalis* growth in planktonic culture (see Fig. S1 in the supplemental material), indicating that iron-mediated augmentation of *E. faecalis* growth is a biofilm-specific phenotype. For detailed visualization of *E. faecalis* cell distribution and biofilm architecture properties, we created three-dimensional (3D) reconstructions of high-magnification CLSM stacks (Fig. 1b). At 18 h, 37°C *E. faecalis* biofilm forms a flat monolayer in the normal medium as reported previously (22, 23). In contrast, *E. faecalis* biofilm is thicker and the bacterial cells are distributed throughout the biofilm when iron is supplemented. We therefore hypothesized that *E. faecalis* gains a metabolic advantage by the supplementation of iron, which in turn affects growth rate. We reasoned that at a reduced temperature, the *E. faecalis* growth rate would decrease and possibly modulate the dependence on iron supplementation. At 120 h, *E. faecalis* grown at 22°C forms a sparse monolayer biofilm in normal medium; however, the biofilm expands to a depth of greater than 24 μm (the image resolution limit of CLSM) and increased cell density in iron-supplemented medium. To evaluate morphological changes in *E. faecalis* cells or the biofilm matrix, we analyzed biofilm cells grown in flow cells by transmission electron microscopy (TEM). We observed typical diplococ-

Downloaded from mbio.asm.org on May 14, 2018 - Published by mbio.asm.org

cal *E. faecalis* in the normal biofilm cells with an abundance of extracellular fibrous material in the matrix (Fig. 2a, b, and c). Constituents of the *E. faecalis* biofilm matrix are not well characterized; however, *E. faecalis* can actively secrete extracellular DNA (eDNA) in biofilms, and DNase treatment can disperse *E. faecalis* biofilms, suggesting that eDNA is a major component of the matrix (24–26). TEM images of the iron-supplemented biofilm are similar to normal biofilm (Fig. 2a, b, and c and S2b), with the exception of electron-dense particles associated with the extracellular fibrous matrix material (Fig. 2d, e, and f and S2f). Using energy-dispersive X-ray spectroscopy (EDS) in a TEM to analyze the same samples, we demonstrated the extracellular electron-dense particles to be enriched in iron (Fig. 2g to m and S2h and i) and hypothesize that these iron deposits, together with the increased biomass observed by CLSM, are important for augmented *E. faecalis* biofilm formation.

Iron-induced *Enterococcus faecalis* growth is biofilm specific, and iron availability impacts the metallome. To determine if redox-active metals other than iron and heme could also augment *E. faecalis* biofilm formation, we performed static biofilm assays via crystal violet (CV) staining in microtiter plates to increase throughput (27). In contrast to continuous-feed flow cell biofilms where we use diluted (10%) medium and 0.2 mM $FeCl_3$ because nutrients are not limiting, we use full-strength medium and 2 mM $FeCl_3$ for microtiter plate biofilms because they are a closed-batch system where nutrients are finite (28). In all biofilm assays, we included abiotic medium controls with metals supplemented to monitor metal precipitation and found that no metals fell out of solution at the concentrations tested in these assays (data not shown). Consistent with *E. faecalis* biofilm augmentation observed when grown in flow cells with 0.2 mM supplemented $FeCl_3$ (Fig. 1a and b), 2 mM $FeCl_3$-enriched medium augmented *E. faecalis* static biofilm growth over time (0 to 120 h) compared to the normal medium (Fig. 3a). The biomass was significantly greater at $FeCl_3$ concentrations of 0.5 to 2 mM (Fig. 3a). Above these concentrations, biomass was also enhanced but not as significantly compared to the nonsupplemented control. We next investigated the capacity of different metal species to augment *E. faecalis* biofilm accumulation and found that supplementation with ferrous sulfate ($FeSO_4$) or ferric sulfate [$Fe_2(SO_4)_3$] also increased *E. faecalis* biofilm growth, whereas ferric citrate and magnesium chloride ($MnCl_2$) had negligible effects on *E. faecalis* biofilm (Fig. 3b). Zinc chloride ($ZnCl_2$) and copper chloride ($CuCl_2$) modestly diminished biofilm formation, suggesting that *E. faecalis* biofilm cells may be more sensitive to zinc- or copper-mediated toxicity. Manganese chloride had a modest augmenting effect on biofilm formation. Heme supplementation at concentrations from 50 to 150 μM also significantly promoted biofilm accumulation and is likely the result of enhanced activity in cytochrome *bd* since heme functions as a cofactor for this enzyme and drives *E. faecalis* to aerobic respiration (29).

TEM analysis (Fig. 2d, e, and f) demonstrated iron deposits in the extracellular biofilm matrix of the iron-supplemented cultures, whereas no extracellular deposits were observed for biofilms supplemented with heme (Fig. S2a to g). We therefore hypothesized that extracellular iron was promoting biofilm growth and that iron concentrations in the *E. faecalis* intracellular metallome would remain stable between the normal and iron-supplemented cultures. We used inductively coupled plasma mass spectrometry (ICP-MS) to quantify the intracellular metallome of *E. faecalis* in the absence (normal) and presence (supplemented) of $FeCl_3$ supplementation (Fig. 3c). While the summed total intracellular metal abundance decreased in the supplemented medium (2,550 ppb) compared to the normal medium (3,360 ppb) (Fig. 3c), intracellular iron in the supplemented samples was greater (750 ppb) than in the normal samples (20 ppb) (Tables S1 and S2). The increase in intracellular iron concentration was coincident with a decrease in intracellular cobalt, aluminum, potassium, magnesium, and zinc when *E. faecalis* was grown in iron-supplemented medium. We also observed an increase in the redox-active metals copper and manganese. Together, these data suggested that iron was substituting for some metals in the supplemented medium and that the substitution was likely to be functionally balanced. Iron, cobalt, and zinc are transition metals that can function as interchangeable ions and can compete with iron for binding

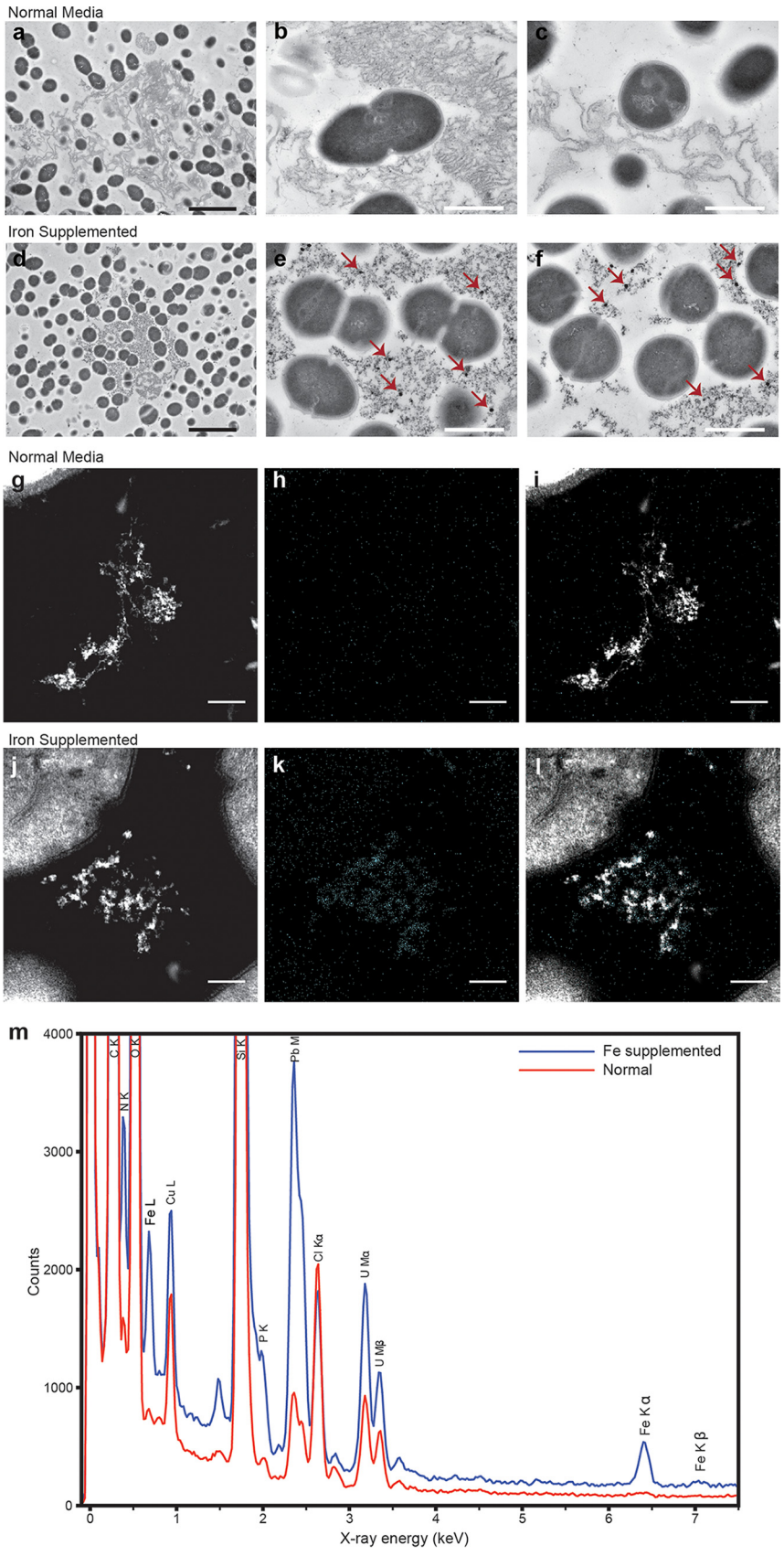

FIG 2 Electron micrographs of the *E. faecalis* biofilm matrix with iron supplementation. Representative images from TEM of *E. faecalis* biofilm from flow cell in normal 10% TSBG (a, b, and c) or 10% TSBG

(Continued on next page)

Downloaded from mbio.asm.org on May 14, 2018 - Published by mbio.asm.org

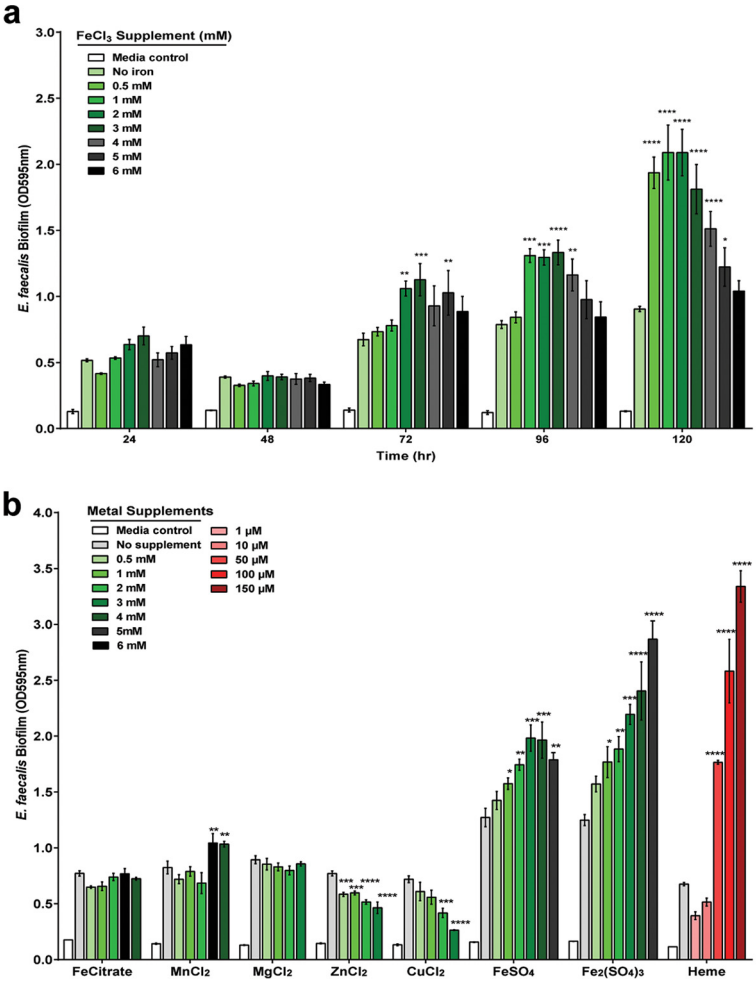

c

Metal	Condition	Mean Conc. +/- SD (ppb)
Al	Supplemented	1197.9122 +/- 462.8346
Al	Normal	2265.4122 +/- 1683.4797
Co	Supplemented	0.0062 +/- 0.0008
Co	Normal	0.0721 +/- 0.0131
Cu	Supplemented	3.0279 +/- 0.4521
Cu	Normal	0.8647 +/- 0.4291
Fe	Supplemented	749.8572 +/- 79.9801
Fe	Normal	20.1940 +/- 16.4766
K	Supplemented	412.8805 +/- 76.8380
K	Normal	717.0068 +/- 181.0022
Mg	Supplemented	180.7860 +/- 28.7930
Mg	Normal	237.1211 +/- 68.0161
Mn	Supplemented	5.0773 +/- 0.7728
Mn	Normal	0.7922 +/- 0.2512
Zn	Supplemented	0.5509 +/- 0.2261
Zn	Normal	115.4938 +/- 7.5407

FIG 3 *E. faecalis* biofilm growth under metal supplementation. (a) Time course of *E. faecalis* biofilm growth in TSBG supplemented with $FeCl_3$. (b) *E. faecalis* biofilm growth at 120 h in TSBG supplemented with metals as indicated. (c) ICP-MS analysis of *E. faecalis* grown in TSBG (normal) and TSBG supplemented with 2 mM $FeCl_3$ (supplemented). (a and b) Data at each time point or metal supplement represent an independent experiment, with the data merged for representation. (a to c) $n = 3$ biological replicates. Statistical significance was determined by two-way analysis of variance with Tukey's test for multiple comparisons. $n = 3$ with four technical replicates. *, $P \leq 0.05$; **, $P \leq 0.01$; ***, $P \leq 0.001$; ****, $P \leq 0.0001$. (a) Statistical analysis was calculated with time set as a repeated measure. (a, b, and c) Error bars represent standard deviations from the mean.

to metalloproteins (30). This may explain the decrease in cobalt and zinc levels. The increase in intracellular iron in the supplemented samples suggests that iron may play an intracellular role in biofilm augmentation. Together with the extracellular electron-dense deposits, iron flux across the membrane may be contributing to biofilm growth. We hypothesized that identifying genes involved in metal acquisition would help determine if intracellular iron was important for iron-enhanced biofilm growth. We examined 21 mutants of uncharacterized *E. faecalis* membrane transport or regulation systems, with homology to previously characterized metal-associated proteins in other bacteria, and measured intracellular metal content by ICP-MS (Tables S1, S2, and S3) (31). However, these mutants did not have significant changes in intracellular iron in the normal or supplemented medium. Because bacterial iron transport systems are

FIG 2 Legend (Continued)
supplemented with 0.2 mM $FeCl_3$ (d, e, and f). In panels a to f, bars represent 2 μm (black) and 0.5 μm (white), and red arrows highlight examples of electron-dense particles. The biofilm matrix from biofilms grown in normal medium (g, h, and i) or with iron supplementation (j, k, and l) was examined by HAADF STEM and EDS mapping at ×300,000 magnification: HAADF STEM (g and j), iron EDS map (h and k), and merged EDS-STEM images (i and l) are shown at ×300,000 magnification. Bars in panels g to l represent 1 μm. The EDS spectra for iron, corresponding to the images, are shown in panel m.

Downloaded from mbio.asm.org on May 14, 2018 - Published by mbio.asm.org

Downloaded from mbio.asm.org on May 14, 2018 - Published by mbio.asm.org

generally expressed under iron limitation, we also tested these mutants in an iron-chelated medium where *E. faecalis* planktonic growth has previously been shown to be growth limited (10) and found that 15 mutants were attenuated for iron uptake when iron was limiting (Table S4). Overall, the ICP-MS analysis has demonstrated modulation of the *E. faecalis* metallome when cultured at different iron concentrations and identified systems involved in metal acquisition. However, this study did not identify any systems involved in iron acquisition in the supplemented medium, suggesting that they are not involved or that there is a large amount of overlapping functionality in iron transport in *E. faecalis*.

Genes involved in *E. faecalis* metabolism contribute to iron-induced biofilm growth. To determine the mechanism underlying iron-enhanced *E. faecalis* biofilm, we screened a near-saturated *E. faecalis* mariner transposon (Tn) library for changes in biofilm formation in medium supplemented with 2 mM $FeCl_3$ (31). Using the CV biofilm assay, we screened the transposon library for mutants displaying either loss or further enhancement of biofilm growth (Fig. S3a). Mutants displaying altered biofilm growth in iron-supplemented medium were also examined for alterations in planktonic growth in normal or supplemented medium, to eliminate mutants with general fitness defects (Fig. S3a). Because we were seeking factors specifically involved in biofilm formation in excess iron, and not general biofilm factors, we performed a secondary biofilm assay to exclude mutants that displayed altered biofilm in both iron-supplemented and normal medium (Fig. S3b to g). The final *E. faecalis* transposon mutants that specifically altered biofilm formation in excess iron included single insertions in *phoH*, *ldh1*, *trxB2*, OG1RF_10589, and an intergenic region (Table S5). The predicted functions for all of the gene products were associated with metabolism functions and membrane transport.

EET to iron occurs in *E. faecalis* biofilm. Dissimilatory metal-reducing bacteria, such as *Shewanella* spp. and *Geobacter* spp., take advantage of extracellular redox-active metals as terminal electron acceptors for respiration by extracellular electron transfer (EET) (32, 33). *Shewanella* spp. and *Geobacter* spp. both have functional iron transport and regulation systems for intracellular iron homeostasis (34, 35). Electroactivity has also been detected in some *Enterococcus* spp. where exogenous redox mediators have been added as supplements (36, 37). Our data indicate that genes involved in energy production, redox control, and membrane transport contributed to iron-augmented biofilm (Table S2). We also observed iron deposits in the biofilm matrix that surrounds the bacterial cell surfaces of iron-enhanced biofilm (Fig. 2d, e, f, k, and m). We therefore hypothesized that the extracellular iron associated with *E. faecalis* biofilm matrix may function as electron sinks during biofilm metabolism, where Fe(III) is reduced to Fe(II) by *E. faecalis*. To test this, we used chronocoulometry to measure EET of *E. faecalis* biofilms grown in electrochemical cells on a carbon screen-printed electrode (SPE) maintained at high oxidative potential. This assay measures the integral of current over time, i.e., the charge transferred to the electrode over time, and therefore monitors in real time whether *E. faecalis* is capable of sustained EET in the presence of oxidized iron. Importantly, electrons are detected only at the electrode surface, and as such, any intracellular iron reduction cannot be measured by chronocoulometry. Chronocoulometry is commonly used to measure the electron transfer process in redox systems (38) and was previously used to measure EET in *Pseudomonas aeruginosa* (39). Using this assay, we observed that *E. faecalis* biofilms grew on the carbon electrode (Fig. S4a and b) and generated extracellular current in iron-supplemented medium, while all abiotic medium controls and *E. faecalis* biofilms grown in normal medium did not yield a current (Fig. 4a). Moreover, extracellular current generation was specific to the addition of iron, because we observed no current upon the addition of the other biofilm-augmenting metal magnesium, manganese, or heme (Fig. S4c). We then tested the five mutants identified through the transposon screen for the generation of extracellular current in the supplemented medium. Only the *ldh1* mutant displayed significantly reduced current compared to the parental strain (Fig. 4a), suggesting that L-lactate dehydrogenase (LDH) was involved in extracellular electron transfer in *E. faecalis*. We

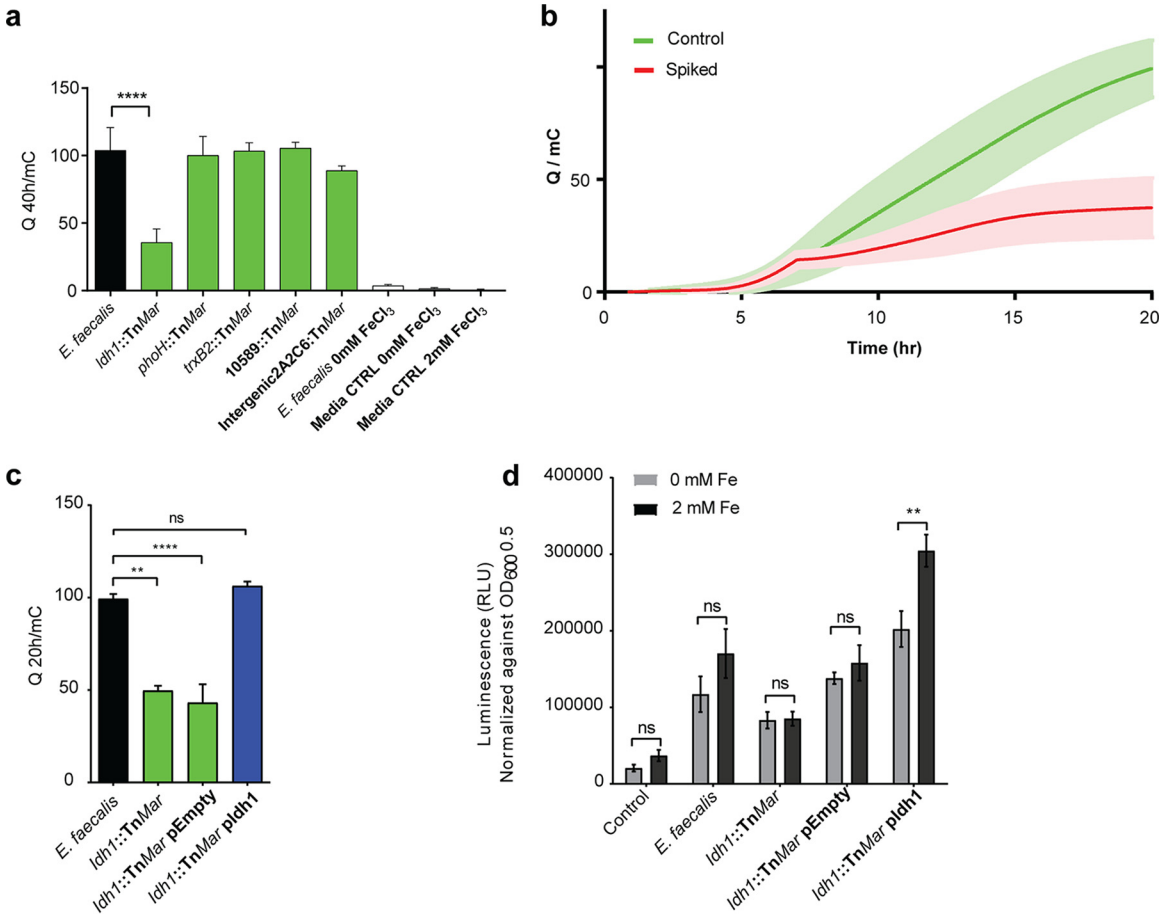

FIG 4 Extracellular electron transfer in *E. faecalis* biofilm. (a) Chronocoulometry current (*Q*) measurement, expressed in millicoulombs, of *E. faecalis* biofilm on a screen-printed electrode over 40 h in TSBG supplemented with 2 mM $FeCl_3$ (supplemented). Abiotic controls and medium controls are indicated. Statistical significance was determined by one-way analysis of variance with Tukey's test for multiple comparisons. $n = 3$ biological replicates. Error bars represent standard deviations from the mean. ****, $P \leq 0.0001$. (b) Chronocoulometry of *E. faecalis* biofilm in iron-supplemented medium with a chelator spike (4 mM 2,2′-dipyridyl) at 7.5 h. Representative data from four independent experiments are shown, where the trend is consistent among all experiments. Statistical significance was determined by a paired two-tailed *t* test; error bars (light green or light red shading) represent standard deviations from the mean. ****, $P \leq 0.0001$. (c) Chronocoulometry current (*Q*) measurement, expressed in millicoulombs, of *E. faecalis* wild-type, *ldh1* mutant, and complemented *ldh1* mutant biofilm on a screen-printed electrode over 40 h in TSBG supplemented with 2 mM $FeCl_3$. Statistical significance was determined by one-way analysis of variance with Tukey's test for multiple comparisons. $n = 3$ biological replicates. Error bars represent standard deviations from the mean. ****, $P \leq 0.0001$. (d) ATP quantification within biofilm grown in TSBG and TSBG supplemented with 2 mM $FeCl_3$ for 24 h. Nisin was included at 5 μg/ml, and erythromycin was included at 300 μg/ml for strains carrying a plasmid. Statistical significance was determined by one-way analysis of variance with Sidak's test for multiple comparisons. $n = 2$ biological replicates. Error bars represent standard errors of the means. **, $P \leq 0.01$; ns, not significant. ATP production was significantly increased for *E. faecalis* when grown in iron-supplemented medium in each of two individual experiments ($P < 0.05$) (data not shown).

complemented the *ldh1* mutant using a nisin-inducible expression plasmid and restored biofilm formation to wild-type levels (Fig. S5). We quantified extracellular current by chronocoulometry for the *ldh1* mutant and the complemented strain and observed that current was also restored to the levels observed in the wild-type strain (Fig. 4c). To validate that extracellular iron was required, we spiked the electrochemical cell with the chelator 2,2′-dipyridyl to sequester iron. In the presence of iron chelation, we observed a significant reduction in current (Fig. 4b), demonstrating that soluble iron was instrumental to the process of EET. To ensure that chelator addition did not give rise to cell death leading to the observed loss of current production, we performed CLSM with live/dead staining to verify that chelation did not alter viability (data not shown). To test whether EET was generating increased energy for the bacterial biofilm, we quantified ATP levels at 24 h (Fig. 4d). We observed a nonsignificant increase in ATP in iron-supplemented medium for the wild-type strain, but not for the *ldh1* mutant, compared to

Downloaded from mbio.asm.org on May 14, 2018 - Published by mbio.asm.org

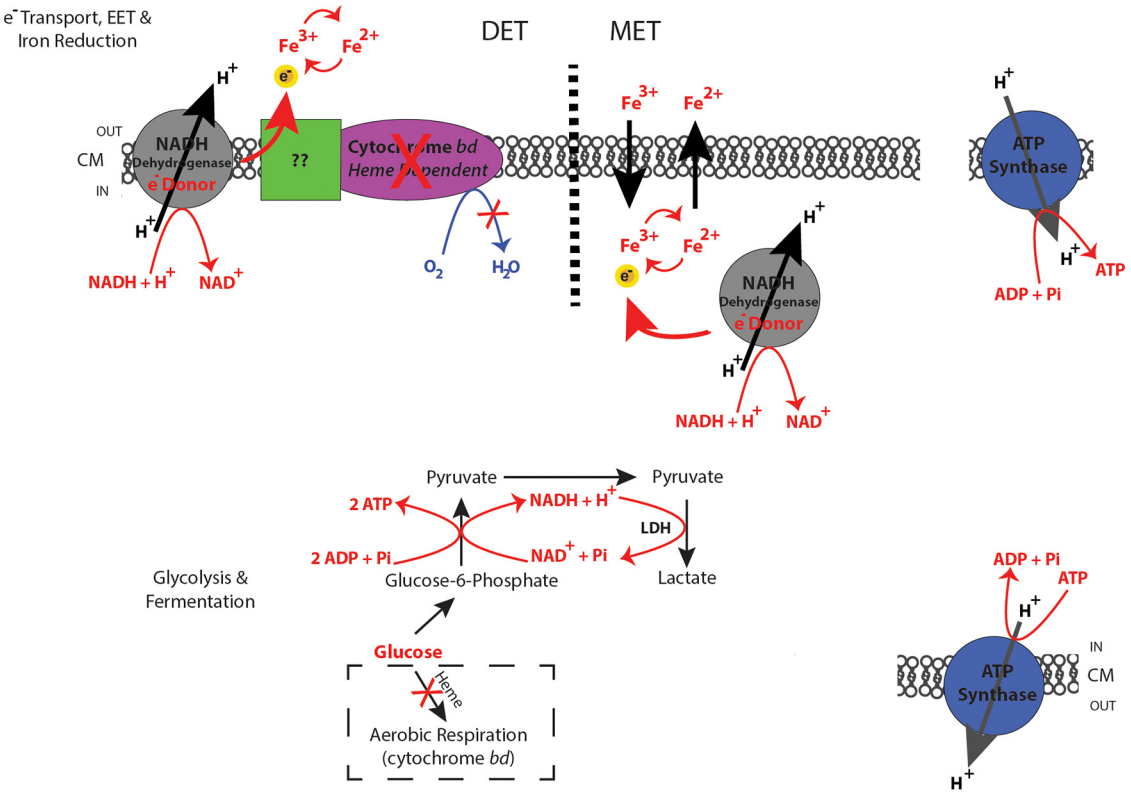

FIG 5 Model for fermentation and EET-dependent respiration metabolism in *E. faecalis* biofilm. Schematic model for *E. faecalis* biofilm metabolism describing EET through DET and MET mechanisms. ATP is generated by proton flow through membrane-integrated ATP synthases. Glycolysis and fermentation are required prior to EET-dependent respiration. This generates the fermentation end products required as the substrates for dehydrogenases acting as electron donors. DET occurs in the absence of heme, where extracellular iron can be reduced and thereby serve as an iron sink for electrons of the respiratory electron transport chain. MET occurs in the absence of heme, when iron is transported intracellularly and reduced, thereafter being exported and serving as an electron mediator/shuttle.

normal medium. The *ldh1*-complemented strain, however, significantly increased ATP levels in iron-supplemented medium compared to the empty-vector control, suggesting that energy was more abundant in iron-supplemented biofilm when *ldh* was present.

Taken together, our results allow us to propose several models for *E. faecalis* biofilm metabolism where EET, using biofilm matrix-associated iron, supports biofilm growth. In the first model (Fig. 5), we propose that in the absence of heme, as was the condition in this study, where cytochrome *bd* is nonfunctional for aerobic respiration, fermentation end products such as lactate can be used as the substrates by LDH to generate a modification of the electron transport chain. We suggest that this dehydrogenase may act as an electron donor transferring electrons to iron in the biofilm matrix and producing greater energy levels to augment biofilm growth. The precise route of electron flow is yet to be determined; however, we propose two possibilities based on data from our study and previous EET mechanism studies (40–47). LDH may act as an electron donor transferring electrons through the cytoplasmic membrane to iron acceptors in the biofilm matrix. As in other bacterial EET systems, direct electron transfer (DET) or mediated electron transfer (MET) mechanisms mediate the transit of electrons to the environment. For *E. faecalis*, this would require involvement of the membrane quinone pool (demethylmenaquinone [DMQ] specifically, since ubiquinone and menaquinone have not been identified in *E. faecalis* [48]) or membrane iron transporters to ultimately use iron in the biofilm matrix for EET and generate greater energy levels. Alternatively, LDH may not directly serve as an electron donor but may act indirectly to influence the expression or function of other mediators of electron transfer during EET.

Downloaded from mbio.asm.org on May 14, 2018 - Published by mbio.asm.org

Downloaded from mbio.asm.org on May 14, 2018 - Published by mbio.asm.org

DISCUSSION

In this study, we characterize a new form of *E. faecalis* biofilm-specific metabolism where iron promotes EET, causing increased energy production and augmented biofilm growth. Although further investigation is needed to understand the physiological relevance of our results, understanding the diversity of metabolic possibilities may be important for understanding how *E. faecalis* colonizes different niches such as the human gastrointestinal tract, where iron is abundant (49), or the environment (50–52). The metabolic versatility of enterococci supports their survival in diverse and complex environments and communities, thus increasing the possibility of dissemination to new niches when iron is present (53).

Our findings demonstrate that *E. faecalis* is electroactive and likely takes advantage of Fe(III)/Fe(II) redox coupling to transfer electrons extracellularly, thus increasing energy production and augmenting biofilm growth. An Fe(III)/Fe(II) oxyhydroxide mixture is likely to represent a portion of the extracellular iron, which could serve to support biofilm growth by functioning as an electron sink (32). To explain this, we propose one model (Fig. 5) in which glycolysis and fermentation proceed prior to EET-dependent respiration to produce pyruvate. Pyruvate then oxidizes to lactate in the presence of LDH, resulting in the flow of electrons to an extracellular electron acceptor. EET can function by both DET, which involves outer membrane *c*-type cytochromes (42), and MET, which takes advantage of microbially produced redox mediators (39, 43, 54, 55). The precise site of EET-mediated iron reduction for *E. faecalis*, either intracellular or extracellular, is not yet known.

Bacteria capable of EET have been shown to mediate electron flow through membrane-embedded DMQ (56). While we did not detect a DMQ pathway mutant in our transposon library screen, this may be due to redundancies inherent in aerobic respiration chains or the substitution of enzyme functions required for DMQ-type molecules (57, 58). Alternatively, LDH could indirectly affect cellular chemistry, or other mediators of electron transfer to promote EET, energy production, and biofilm growth may be at play. Regardless, these findings extend the current knowledge regarding the extent of EET-capable bacterial species and environments, which are primarily viewed in the context of energy recovery in systems such as microbial fuel cells (33).

Gram-negative bacteria represent the majority of characterized EET producers, with a small number of Gram-positive bacteria, such as *Thermincola potens* and *Desulfotomaculum reducens*, characterized as being DET specific (59). Other Gram-positive microorganisms, such as *Corynebacterium* sp. (60) and *E. faecalis* itself, have been shown to produce electricity in microbial fuel cells when artificially supplied with the redox mediators anthraquinone-2,6-disulfonate (AQDS) and riboflavin (37), respectively. *Enterococcus gallinarum* can use iron as an electron acceptor, but the impact on growth was not determined (61). Our work demonstrates that *E. faecalis* achieves augmented growth through a biofilm-specific iron-dependent EET metabolism, and we show that LDH contributes to this phenotype.

E. faecalis and other lactic acid bacteria (LAB) encode the components necessary for aerobic respiration metabolism (62). These are (i) NADH dehydrogenases functioning as electron donors and (ii) a quinone pool to transfer electrons to (iii) the terminal electron acceptor complex cytochrome oxidase (63). The *E. faecalis* cytochrome *bd* enzyme can use oxygen as a terminal electron acceptor only when exogenous sources of its cofactor heme are available (5, 64). *E. faecalis* does not synthesize porphyrin and, in the absence of heme, relies on fermentation. Our experimental assays mimic the absence of heme because it is not present in the growth medium. Our genetic and bioelectrochemical data suggest that *E. faecalis* LDH contributes to EET, in which electrons are transferred to biofilm matrix-associated iron sinks. Dehydrogenases transfer hydride from one substrate to another in a reversible reaction that relies on the interconversion of NADH and NAD^+. Previous studies suggest that, in contrast to most bacterial species that rely on the tricarboxylic acid (TCA) cycle to produce NADH, LAB instead rely on fermentation for its production (65). Fermentation therefore is a necessary metabolic phase prior to

Downloaded from mbio.asm.org on May 14, 2018 - Published by mbio.asm.org

the use of EET to support biofilm metabolism. In *Lactococcus lactis*, a fermenting LAB strain, activation of respiration metabolism in the absence of heme and oxygen reduction occurs by copper reduction via the menaquinone pool (66). This supports our finding that extracellular iron is functioning as an electron acceptor and/or mediator that can activate respiration metabolism in the absence of heme and cytochrome *bd* activity.

Our biofilm data demonstrate an iron-specific *E. faecalis* enhanced biofilm growth response, with only $FeCl_3$, heme, $FeSO_4$, and $Fe_2(SO_4)_3$ stimulating the response. Heme availability enables respiration through cytochrome *bd* activity in the presence of oxygen (29). $FeSO_4$ and $Fe_2(SO_4)_3$ are more labile to oxidative changes and precipitation, required for metabolically driven iron reduction, than the more soluble ferric citrate, which does not enhance biofilm growth, suggesting that the mechanism governing enhanced biofilm growth is most specific to $FeCl_3$.

E. faecalis can flourish in iron-limited environments and tolerate oxidative stress which can be induced by a high-iron environment, contrasting with many other bacterial species where iron is an essential growth nutrient and requires strict iron homeostasis (67). Nonetheless, our ICP-MS analysis shows that iron represents a large proportion of the *E. faecalis* metallome under normal conditions. The modulation of the *E. faecalis* metallome with changes in conditions of either iron limitation or abundance suggests alternative roles for this metal. The absence of detectable iron in the *E. faecalis* mutants with disruptions in genes predicted to encode iron transport and regulatory components, analyzed by ICP-MS under iron limitation, suggests that these gene products function in iron acquisition. Previous transcriptomic studies of planktonic cultures propose roles for *E. faecalis* transport systems in iron acquisition; however, our ICP-MS analysis is the first functional characterization of these systems (11, 12). Manganese has been reported to substitute for iron as a cofactor in essential cellular reactions of LAB species; however, our data demonstrate that iron represents a greater proportion of the *E. faecalis* metallome than manganese under normal and iron-supplemented conditions (7, 8). The ICP-MS analysis equally highlights that a number of other metals, such as zinc, potassium, and magnesium, are abundant. Cobalt and zinc are important metals for bacterial growth, and we have identified a number of genes governing cobalt and zinc utilization in *E. faecalis* (68). While the intracellular iron levels in the iron-supplemented medium were greater than that under the normal condition, no iron transport systems could be identified under these conditions. However, overlapping functionality in nutrient transport is a common strategy for bacteria, and so single-gene mutations may not be sufficient under this condition. Intracellular storage of iron may be strategic in anticipation of acceptor-limited conditions under which this metal can be deposited extracellularly.

Colonization and persistence in host niches and the environment require adaptability in the exploitation of available resources for energy production and growth. Our work highlights a new form of metabolism where, in the absence of heme, components of respiration can be utilized for EET using extracellular iron. This deeper understanding of mechanisms governing biofilm metabolism in humans and clinically relevant bacterial species will enhance approaches to modify or eradicate these reservoirs.

MATERIALS AND METHODS

Bacterial strains and growth conditions. *Enterococcus faecalis* OG1RF (ATCC 47077) (69) was grown in brain heart infusion broth (BHI) and cultured at 37°C under static conditions. *E. faecalis* SD234 is an OG1RF strain derivative harboring a constitutively expressed *gfp* gene (70). Overnight cultures were normalized to 2×10^8 to 4×10^8 CFU/ml in phosphate-buffered saline (PBS), equivalent to an optical density at 600 nm (OD_{600}) of 0.7 for *E. faecalis*. For planktonic and biofilm assays, bacteria were cultured at 37°C (under 200-rpm orbital shaking or static conditions, respectively) with tryptone soy broth supplemented with 10 mM glucose (TSBG) and solidified with 1.5% agar when appropriate (Oxoid Technical no. 3). Planktonic assay mixtures were inoculated from the normalized stocks to a starting CFU of 2×10^5 to 4×10^5 CFU/ml. *E. faecalis* strains harboring pMSP3535 (source, Gary M. Dunny; Addgene plasmid 46886) or pMSP3535::*ldh1* (source, Axel Hartke [71]) were selected for with 300 μg/ml erythromycin and induced with 5-μg/ml nisin-supplemented BHI. BHI was supplied by Becton, Dickinson and Company, Franklin Lakes, NJ. TSB and agar were supplied by Oxoid Inc., Ontario, Canada. Metals for supplementation were added during medium preparation. Ferric citrate hydrate (≥98%); magnesium

Downloaded from mbio.asm.org on May 14, 2018 - Published by mbio.asm.org

chloride, anhydrous (≥98%); copper chloride dihydrate (≥99%); ferrous sulfate heptahydrate (≥99%); ferric sulfate hydrate (≥97%); ferric chloride, anhydrous (≥99%); heme (≥90%); and the chelator 2,2′-dipyridyl (≥99%) were all supplied by Sigma-Aldrich, St. Louis, MO, USA. Manganese chloride tetrahydrate and zinc chloride were supplied by Merck Millipore (Singapore).

Biofilm assay. Bacterial cultures were normalized as described above and inoculated at 1.6×10^6 to 3.2×10^6 CFU/200-μl microtiter well in TSBG in a 96-well flat-bottom transparent microtiter plate (Thermo Scientific, Waltham, MA) and incubated at 37°C under static conditions. Uninoculated medium controls supplemented with metals to the highest concentration relevant to the assay were included to check for supplemented metal precipitation. Supernatants were discarded, and the microtiter plate was washed twice with PBS. To stain surface-adherent bacteria, 200 μl of crystal violet solution at 0.1% (wt/vol) (Sigma-Aldrich, St. Louis, MO, USA) was added to each well and incubated at 4°C for 30 min. This solution was discarded, and the microtiter plate was washed twice with PBS followed by crystal violet solubilization with 200 μl per well ethanol-acetone (4:1) for 45 min at room temperature. The intensity of crystal violet staining was measured by absorbance at 595 nm (OD_{595}) using a Tecan Infinite 200 Pro spectrophotometer (Tecan Group Ltd., Männedorf, Switzerland).

Flow cell biofilm assay. Flow cell biofilm studies were performed as previously described with minor modifications (72). Bacterial cultures were normalized to 2×10^6 to 4×10^6 CFU/ml in PBS, and 250 μl of this stock was injected through the Stovall flow cell system inlet silicon tube connected to the flow cell chamber. This inoculation was performed when the system flow was halted by clamping both the inlet and outlet silicon tubes. The chamber was inverted for 1 h to facilitate bacterial adherence to the glass slide surface. The flow cell system was then reset and unclamped, and the medium feed was set to 4.5 ml/h.

Transposon library screen. The cryogenically stocked, 96-well-format *E. faecalis* OG1RF mariner transposon library consisted of 14,978 individual mutants (31). This library was cultured using a cryoreplicator (Adolf Kühner AG) to inoculate DeepWell blocks (Greiner Bio-One) containing 1 ml BHI medium for overnight incubation at 37°C with shaking at 220 rpm. Cultures were normalized to an OD_{600} of 0.1 (2×10^8 to 4×10^8 CFU/ml) in PBS with the Tecan Infinite 200 Pro spectrophotometer (Tecan Group Ltd., Switzerland) using a 96-well microtiter plate. The primary screen of the library was performed by inoculating a microtiter well with 1.6×10^6 to 3.2×10^6 CFU/200 μl in TSBG medium supplemented with 2 mM $FeCl_3$. The microtiter plates were then incubated at 37°C, statically, inside a moistened chamber to prevent evaporation of medium. Biofilm was quantified by crystal violet staining as described above. Mutants with either reduction or further enhancement of biofilm signal compared to wild-type controls were then validated using two independent biological replicates for each mutant in TSBG biofilm assays. This primary validation was followed by a planktonic growth validation in TSBG and TSBG medium supplemented with 2 mM $FeCl_3$. A secondary validation using three independent biological replicates for each mutant was performed in biofilm assays with TSBG and TSBG medium supplemented with 2 mM $FeCl_3$ to eliminate any mutants exhibiting defects in biofilm formation under normal conditions. Mutants harboring multiple transposon (Tn) insertions were excluded from the screen.

Mapping Tn insertions. Genomic DNA (gDNA) was extracted using the Wizard genomic DNA purification kit (Promega) from transposon mutants that were not originally mapped. The gDNA was quantified and assessed for nucleic acid quality by the Qubit highly sensitive double-stranded DNA (dsDNA) assay (Invitrogen) and a NanoDrop spectrophotometer. Sequencing was performed using an Illumina MiSeq sequencer. *De novo* reads were assembled using CLC Genomics Workbench version 8.0 and *E. faecalis* OG1RF as a template. The Tn insertion site was identified by BLAST using the mariner transposon sequence and identification of the flanking genomic sequence. Transposon mutant strains were named to include library location information, gene name, or intergenic information, followed by "TnMar." For example, (4.2A1 F1)10589:TnMar indicates the transposon mutant for OG1RF_10589 located in block 4.2A1 of the library in position F1 of the microtiter plate.

Electrochemical setup and analysis. Screen-printed electrodes (SPEs) (model DRP-C110; DropSens, Spain) consisting of a carbon working electrode, carbon counter electrode, and Ag pseudoreference electrode were controlled by a multichannel potentiostat (VSP; Bio-Logic, France) in an electrochemical cell of 9-ml working volume sealed with a Teflon cap. Chronocoulometry was used to characterize the electrochemical activity of live microbial cultures by measuring the charge *Q* passed over the course of growth, with *Q* (millicoulombs) at 40 h used for comparison. During chronocoulometry, the working electrode was maintained at 200 mV versus the Ag pseudoreference electrode of the SPE. This potential was chosen as it is high enough to reoxidize Fe(II) to Fe(III) while being low enough to avoid damaging the bacteria. By applying a set potential to an electrode acting as an electron acceptor, the extracellular current generated can be tracked with time, the integral of which represents the total charge passed. By looking at the charge passed at a fixed time, the electroactivity of a culture/mutant, etc., can be established. Bacterial stocks of 2×10^8 to 4×10^8 CFU/ml for electrochemical experiments were prepared as described above, and electrochemical cells were inoculated to 2×10^5 to 4×10^5 CFU/ml. All electrochemical experiments were conducted at 37°C using TSBG medium supplemented with 2 mM $FeCl_3$ unless otherwise stated. The iron chelator 2,2′-dipyridyl (Sigma-Aldrich, USA) was spiked in selected experiments to quench EET.

Electrode biofilm biomass quantification. Biofilm biomass was analyzed by CLSM directly from screen-printed electrodes with 5 individual z-stack images per biological replicate. Images were acquired using an LSM 780 confocal microscope (Zeiss, Germany) equipped with a 20×/0.8 Plan-Apochromat objective. Viability staining was performed using 5 ml of 200 μM propidium iodide (PI) and 33.4 μM SYTO 9 nucleic acid incubated in the dark for 15 min. After staining, the screen-printed electrodes were washed with 5 ml of 1× phosphate-buffered saline (PBS) twice, mounted inverted on the glass slide, and viewed

Downloaded from mbio.asm.org on May 14, 2018 - Published by mbio.asm.org

using an LSM 780 confocal microscope. Imaging of propidium iodide-stained cells was performed using excitation/emission wavelengths at 561 nm and 633 nm, respectively, while SYTO9 nucleic acid-stained cells were imaged using excitation/emission wavelengths at 488 nm and 500 nm, respectively. Image analysis was performed using Carl Zeiss microimaging software. Analysis of biomass was performed using Imaris software.

Thin-section transmission electron microscopy (TEM). Biofilms were grown using the flow cell protocol or the standard biofilm protocol described above, but with the latter using a 6-well plate. The flow cell biofilm was resuspended in a 2% paraformaldehyde-2.5% glutaraldehyde solution (Polysciences, Warrington, PA) in 100 mM PBS (pH 7.4) for 1 h at room temperature. The samples were then embedded in 2% low-melting-point agarose, washed in PBS, and postfixed in 1% osmium tetroxide for 1 h. Samples were rinsed extensively in distilled water (dH_2O) prior to en bloc staining with 1% aqueous uranyl acetate (Ted Pella, Inc., Redding, CA) for 1 h. Following several rinses in dH_2O, samples were dehydrated in a graded series of ethanol and embedded in Eponate 12 resin (Ted Pella, Inc., Redding, CA). Sections of 95 nm were cut with a Leica Ultracut UCT ultramicrotome (Leica Microsystems, Inc., Bannockburn, IL, USA), stained with uranyl acetate and lead citrate, and viewed on a JEOL 1200 EX transmission electron microscope (JEOL USA, Inc., Peabody, MA).

Energy-dispersive X-ray spectroscopy (EDS) TEM. Samples were prepared as described above for TEM and viewed on an aberration-corrected JEOL ARM 200 cold field-emission gun transmission electron microscope in high-angle annular dark-field scanning transmission (HAADF STEM) mode using spot size 6. The sample was held in a JEOL Be double tilt holder tilted by about 12° toward the X-ray detector. STEM images were collected using a JEOL annular dark-field detector on a Gatan Digiscan with 2,048 by 2,048 pixels and a dwell time of 10 μs. Energy-dispersive X-ray maps were collected using an Oxford Aztec system with an 0.7-sr collection solid angle by scanning the beam with multiple frames over a period of about 5 min at a resolution of 512 by 512 pixels.

ATP quantification. Biofilms were grown in 6-well microtiter plates at 37°C for 24 h under static conditions as described above. Spent medium was removed, and the adherent biofilm was washed with 1 ml of 1× PBS, disrupted into a single-cell suspension, and normalized to an OD of 0.5. One hundred microliters of normalized biofilm sample was added to 100 μl of prepared BacTiter-Glo reagent from the BacTiter-Glo microbial cell viability assay kit (Promega) and incubated at room temperature for 5 min before measuring luminescence using a Tecan Infinite 200 Pro spectrophotometer (Tecan Group Ltd., Männedorf, Switzerland). An integration time of 0.25 to 1 s per well was used.

Confocal laser scanning microscopy and 3D reconstruction. Biofilm morphology, biomass, and cell distribution were analyzed by CLSM directly from flow cell chamber glass microscope slides at three separate locations (inlet, middle, and outlet areas) with 3 individual z-stack images per technical replicate. Images were acquired using an LSM 780 confocal microscope (Zeiss, Germany) equipped with a 20×/0.8 Plan-Apochromat objective and controlled by ZEN software. Samples were illuminated with a 488-nm argon laser line, and the GFP emitted fluorescence was collected in the 507- to 535-nm range. Optical sections (425 by 425 μm) were collected every 5 μm through the entire biofilm thickness, and the signal from each section was averaged 2 to 4 times. Fiji software (73) was used for further processing (level adjustment and stack reslice). For the 3D biofilm reconstructions, optical slices (85 by 85 μm) were acquired with a 63×/1.4 Plan-Apochromat oil immersion lens every 0.3 μm through the entire biofilm thickness or until loss of the fluorescence signal (due to light scattering, absorption, and possible fluorescence quenching of thick iron-supplemented biofilms). The center of mass for each cell in 3D space was found using MosaicSuite for Fiji (74), and then coordinates were filtered in R (75). To visualize the biofilm matrix and spatial organization, coordinates were plotted as spheres with cell size diameter and color-coded *z*-depth.

ICP-MS. *E. faecalis* cultures were prepared as previously described with minor modifications (76). Overnight cultures were normalized as described above, and 1×10^5 to 2×10^5 CFU/well was inoculated into DeepWell blocks (Greiner Bio-One) containing 2 ml TSBG medium and incubated overnight at 37°C under static conditions. Three biological replicates with five technical replicates were prepared for each *E. faecalis* strain, and following incubation, the technical replicates were pooled prior to preparation for ICP-MS. Harvested cell pellets were washed with 10 mM EDTA (Ambion Thermo Fisher Scientific, USA) prepared in liquid chromatography-mass spectrometry (LC-MS)-grade dH_2O (Sigma-Aldrich, St. Louis, MO, USA) and washed three times with LC-MS-grade dH_2O. Cells were then concentrated to 2×10^8 to 4×10^8 CFU/ml in LC-MS-grade dH_2O. Each cell pellet was digested in 500 μl of 69% nitric acid and 250 μl of 31% hydrogen peroxide. Following sample digestion, all the samples were diluted with LC-MS-grade dH_2O to a 2% (wt/vol) nitric acid concentration in the final solution.

An Agilent 7700 series model ICP-MS system (Agilent, Santa Clara, CA) was used for simultaneous determination of selected elements (Mg, Al, P, K, Ca, V, Cr, Mn, Fe, Co, Ni, Cu, and Zn) in prepared *E. faecalis* samples. Prior to sample measurement and quantification, stock solutions of a multielement calibration standard (Inorganic Ventures, VA, USA) were serially diluted (0 μg/liter to 1,000 μg/liter) and run on the system. For each measurement (standards, samples, blanks, and quality controls), addition of internal standard (Sc; 100 mg/liter, Agilent, USA) was performed to correct for physical matrix effects. Blanks were determined together with samples for every run, and the mean for three runs was determined for each sample. Full quantitative analysis was performed against calibration standards for each element. Quality control samples (multielement calibration solution; 100 μl) were inserted and run at regular intervals during the experiment to ensure reliability of the data and to eliminate signal drift or interference.

For statistical analysis, 10 metals were measured for 22 phenotypes (*E. faecalis* OG1RF wild type and 21 mutants) under three nutrient conditions, with 3 biological replicates for each mutant and under each

condition. During the ICP-MS run, 3 technical replicates were measured from each sample, which were then averaged and used for statistical analysis. The concentration of the metals in a blank control (500 μl of 69% nitric acid and 250 μl of 31% hydrogen peroxide) was subtracted from the concentration of metals in the samples. Metals whose levels were below the detection limit were coded as not detected. For statistical analysis, metal concentrations were normalized using log base 10 transformation. To test differences between the metal levels in mutants and the control under each nutrient condition, Welch's two-sample *t* tests were performed in R using the t.test function, with correction for multiple comparisons made using the Benjamini-Hochberg procedure.

SUPPLEMENTAL MATERIAL

Supplemental material for this article may be found at https://doi.org/10.1128/mBio.00626-17.

FIG S1, TIF file, 1.9 MB.
FIG S2, JPG file, 1.9 MB.
FIG S3, PDF file, 0.2 MB.
FIG S4, PDF file, 0.4 MB.
FIG S5, TIF file, 1.6 MB.
TABLE S1, XLSX file, 0.02 MB.
TABLE S2, XLSX file, 0.02 MB.
TABLE S3, XLSX file, 0.02 MB.
TABLE S4, XLSX file, 0.01 MB.
TABLE S5, DOCX file, 0.01 MB.

ACKNOWLEDGMENTS

This work was supported by the National Research Foundation and Ministry of Education Singapore under its Research Centre of Excellence Programme, by the National Research Foundation under its Singapore NRF Fellowship program (NRF-NRFF2011-11), and by the Ministry of Education Singapore under its tier 2 program (MOE2014-T2-2-124).

We thank Kenneth Beckman (University of Minnesota) and colleagues for sequencing of the *E. faecalis* transposon library and Wandy Beatty (Washington University in St. Louis) for performing TEM. We thank SCELSE members Sumitra Debina Mitra, Irina Afonina, Shu Sin Chng, Hans-Kurt Fleming, Scott Rice, and Staffan Kjelleberg, as well as Jeff Gralnick (University of Minnesota), for their critical assessment of the manuscript. The transmission electron microscopy EDS analysis was performed at the Facility for Analysis, Characterization, Testing and Simulation (FACTS), Nanyang Technological University, Singapore.

D.K. conceptualized the study. D.K., L.N.L., E.M., and K.A.K. designed the experiments, analyzed data, and prepared the manuscript. D.K. and L.N.L. performed biofilm experiments and analyzed data. A.M. analyzed confocal data and generated 3D reconstruction models. D.K. and S.P. performed the ICP-MS experiments. Y.S. and S.P.N. performed and analyzed mass spectrometry experiments. S.U. and R.B.H.W. analyzed metabolomics data. D.K., L.E.D., L.N.L., P.M.L., and E.M. performed the electrochemistry experiments and analyzed data. L.N.L and C.B.B. performed EDS TEM. J.L.D. and G.M.D. provided the transposon library. All authors reviewed the manuscript.

REFERENCES

1. Hufnagel M, Liese C, Loescher C, Kunze M, Proempeler H, Berner R, Krueger M. 2007. Enterococcal colonization of infants in a neonatal intensive care unit: associated predictors, risk factors and seasonal patterns. BMC Infect Dis 7:107. https://doi.org/10.1186/1471-2334-7-107.
2. Sekirov I, Russell SL, Antunes LC, Finlay BB. 2010. Gut microbiota in health and disease. Physiol Rev 90:859–904. https://doi.org/10.1152/physrev.00045.2009.
3. Flemming HC, Wingender J, Szewzyk U, Steinberg P, Rice SA, Kjelleberg S. 2016. Biofilms: an emergent form of bacterial life. Nat Rev Microbiol 14:563–575. https://doi.org/10.1038/nrmicro.2016.94.
4. Paganelli FL, Willems RJ, Leavis HL. 2012. Optimizing future treatment of enterococcal infections: attacking the biofilm? Trends Microbiol 20:40–49. https://doi.org/10.1016/j.tim.2011.11.001.
5. Winstedt L, Frankenberg L, Hederstedt L, von Wachenfeldt C. 2000. Enterococcus faecalis V583 contains a cytochrome bd-type respiratory oxidase. J Bacteriol 182:3863–3866. https://doi.org/10.1128/JB.182.13.3863-3866.2000.
6. Weinberg ED. 1997. The Lactobacillus anomaly: total iron abstinence. Perspect Biol Med 40:578–583. https://doi.org/10.1353/pbm.1997.0072.
7. Bruyneel B, vande Woestyne M, Verstraete W. 1989. Lactic-acid bacteria—microorganisms able to grow in the absence of available iron and copper. Biotechnol Lett 11:401–406. https://doi.org/10.1007/BF01089472.
8. Marcelis JH, den Daas-Slagt HJ, Hoogkamp-Korstanje JA. 1978. Iron requirement and chelator production of staphylococci, Streptococcus faecalis and enterobacteriaceae. Antonie Leeuwenhoek 44:257–267. https://doi.org/10.1007/BF00394304.
9. Archibald F. 1986. Manganese: its acquisition by and function in the

Downloaded from mbio.asm.org on May 14, 2018 - Published by mbio.asm.org

lactic acid bacteria. Crit Rev Microbiol 13:63–109. https://doi.org/10.3109/10408418609108735.
10. Keogh D, Tay WH, Ho YY, Dale JL, Chen S, Umashankar S, Williams RBH, Chen SL, Dunny GM, Kline KA. 2016. Enterococcal metabolite cues facilitate interspecies niche modulation and polymicrobial infection. Cell Host Microbe 20:493–503. https://doi.org/10.1016/j.chom.2016.09.004.
11. Vebø HC, Snipen L, Nes IF, Brede DA. 2009. The transcriptome of the nosocomial pathogen Enterococcus faecalis V583 reveals adaptive responses to growth in blood. PLoS One 4:e7660. https://doi.org/10.1371/journal.pone.0007660.
12. Vebø HC, Solheim M, Snipen L, Nes IF, Brede DA. 2010. Comparative genomic analysis of pathogenic and probiotic Enterococcus faecalis isolates, and their transcriptional responses to growth in human urine. PLoS One 5:e12489. https://doi.org/10.1371/journal.pone.0012489.
13. Verneuil N, Mazé A, Sanguinetti M, Laplace JM, Benachour A, Auffray Y, Giard JC, Hartke A. 2006. Implication of (Mn)superoxide dismutase of Enterococcus faecalis in oxidative stress responses and survival inside macrophages. Microbiology 152:2579–2589. https://doi.org/10.1099/mic.0.28922-0.
14. Riboulet E, Verneuil N, La Carbona S, Sauvageot N, Auffray Y, Hartke A, Giard JC. 2007. Relationships between oxidative stress response and virulence in Enterococcus faecalis. J Mol Microbiol Biotechnol 13:140–146. https://doi.org/10.1159/000103605.
15. Andrews SC, Robinson AK, Rodríguez-Quiñones F. 2003. Bacterial iron homeostasis. FEMS Microbiol Rev 27:215–237. https://doi.org/10.1016/S0168-6445(03)00055-X.
16. Alexander J, Kowdley KV. 2009. HFE-associated hereditary hemochromatosis. Genet Med 11:307–313. https://doi.org/10.1097/GIM.0b013e31819d30f2.
17. Cao A, Galanello R. 2010. Beta-thalassemia. Genet Med 12:61–76. https://doi.org/10.1097/GIM.0b013e3181cd68ed.
18. Fossati M, Cappelli B, Biral E, Chiesa R, Biffi A, Ossi C, Moro M, Cirillo DM, Clementi M, Soliman C, Ciceri F, Roncarolo MG, Fumagalli L, Marktel S. 2010. Fatal vancomycin- and linezolid-resistant Enterococcus faecium sepsis in a child undergoing allogeneic haematopoietic stem cell transplantation for beta-thalassaemia major. J Med Microbiol 59:839–842. https://doi.org/10.1099/jmm.0.018598-0.
19. Buhnik-Rosenblau K, Moshe-Belizowski S, Danin-Poleg Y, Meyron-Holtz EG. 2012. Genetic modification of iron metabolism in mice affects the gut microbiota. Biometals 25:883–892. https://doi.org/10.1007/s10534-012-9555-5.
20. Lee T, Clavel T, Smirnov K, Schmidt A, Lagkouvardos I, Walker A, Lucio M, Michalke B, Schmitt-Kopplin P, Fedorak R, Haller D. 2017. Oral versus intravenous iron replacement therapy distinctly alters the gut microbiota and metabolome in patients with IBD. Gut 66:863–871. https://doi.org/10.1136/gutjnl-2015-309940.
21. Kopáni M, Miglierini M, Lančok A, Dekan J, Čaplovicová M, Jakubovský J, Boča R, Mrazova H. 2015. Iron oxides in human spleen. Biometals 28:913–928. https://doi.org/10.1007/s10534-015-9876-2.
22. Dale JL, Cagnazzo J, Phan CQ, Barnes AM, Dunny GM. 2015. Multiple roles for Enterococcus faecalis glycosyltransferases in biofilm-associated antibiotic resistance, cell envelope integrity, and conjugative transfer. Antimicrob Agents Chemother 59:4094–4105. https://doi.org/10.1128/AAC.00344-15.
23. Seneviratne CJ, Yip JW, Chang JW, Zhang CF, Samaranayake LP. 2013. Effect of culture media and nutrients on biofilm growth kinetics of laboratory and clinical strains of Enterococcus faecalis. Arch Oral Biol 58:1327–1334. https://doi.org/10.1016/j.archoralbio.2013.06.017.
24. Barnes AM, Ballering KS, Leibman RS, Wells CL, Dunny GM. 2012. Enterococcus faecalis produces abundant extracellular structures containing DNA in the absence of cell lysis during early biofilm formation. mBio 3:e00193-12. https://doi.org/10.1128/mBio.00193-12.
25. Thomas VC, Hiromasa Y, Harms N, Thurlow L, Tomich J, Hancock LE. 2009. A fratricidal mechanism is responsible for eDNA release and contributes to biofilm development of Enterococcus faecalis. Mol Microbiol 72:1022–1036. https://doi.org/10.1111/j.1365-2958.2009.06703.x.
26. Guiton PS, Hung CS, Kline KA, Roth R, Kau AL, Hayes E, Heuser J, Dodson KW, Caparon MG, Hultgren SJ. 2009. Contribution of autolysin and sortase A during Enterococcus faecalis DNA-dependent biofilm development. Infect Immun 77:3626–3638. https://doi.org/10.1128/IAI.00219-09.
27. O'Toole GA. 2011. Microtiter dish biofilm formation assay. J Vis Exp (47):2437. https://doi.org/10.3791/2437.
28. Salli KM, Ouwehand AC. 2015. The use of in vitro model systems to study dental biofilms associated with caries: a short review. J Oral Microbiol 7:26149. https://doi.org/10.3402/jom.v7.26149.
29. Borisov VB, Gennis RB, Hemp J, Verkhovsky MI. 2011. The cytochrome bd respiratory oxygen reductases. Biochim Biophys Acta 1807:1398–1413. https://doi.org/10.1016/j.bbabio.2011.06.016.
30. Foster AW, Osman D, Robinson NJ. 2014. Metal preferences and metallation. J Biol Chem 289:28095–28103. https://doi.org/10.1074/jbc.R114.588145.
31. Kristich CJ, Nguyen VT, Le T, Barnes AM, Grindle S, Dunny GM. 2008. Development and use of an efficient system for random mariner transposon mutagenesis to identify novel genetic determinants of biofilm formation in the core Enterococcus faecalis genome. Appl Environ Microbiol 74:3377–3386. https://doi.org/10.1128/AEM.02665-07.
32. Shi L, Dong H, Reguera G, Beyenal H, Lu A, Liu J, Yu HQ, Fredrickson JK. 2016. Extracellular electron transfer mechanisms between microorganisms and minerals. Nat Rev Microbiol 14:651–662. https://doi.org/10.1038/nrmicro.2016.93.
33. Logan BE. 2009. Exoelectrogenic bacteria that power microbial fuel cells. Nat Rev Microbiol 7:375–381. https://doi.org/10.1038/nrmicro2113.
34. Embree M, Qiu Y, Shieu W, Nagarajan H, O'Neil R, Lovley D, Zengler K. 2014. The iron stimulon and fur regulon of Geobacter sulfurreducens and their role in energy metabolism. Appl Environ Microbiol 80:2918–2927. https://doi.org/10.1128/AEM.03916-13.
35. Yang Y, Harris DP, Luo F, Wu L, Parsons AB, Palumbo AV, Zhou J. 2008. Characterization of the Shewanella oneidensis Fur gene: roles in iron and acid tolerance response. BMC Genomics 9(Suppl 1):S11. https://doi.org/10.1186/1471-2164-9-S1-S11.
36. Pankratova G, Hasan K, Leech D, Hederstedt L, Gorton L. 2017. Electrochemical wiring of the Gram-positive bacterium Enterococcus faecalis with osmium redox polymer modified electrodes. Electrochem Commun 75:56–59. https://doi.org/10.1016/j.elecom.2016.12.010.
37. Zhang E, Cai Y, Luo Y, Piao Z. 2014. Riboflavin-shuttled extracellular electron transfer from Enterococcus faecalis to electrodes in microbial fuel cells. Can J Microbiol 60:753–759. https://doi.org/10.1139/cjm-2014-0389.
38. Aeschbacher M, Sander M, Schwarzenbach RP. 2010. Novel electrochemical approach to assess the redox properties of humic substances. Environ Sci Technol 44:87–93. https://doi.org/10.1021/es902627p.
39. Wang Y, Kern SE, Newman DK. 2010. Endogenous phenazine antibiotics promote anaerobic survival of Pseudomonas aeruginosa via extracellular electron transfer. J Bacteriol 192:365–369. https://doi.org/10.1128/JB.01188-09.
40. Gorby YA, Yanina S, McLean JS, Rosso KM, Moyles D, Dohnalkova A, Beveridge TJ, Chang IS, Kim BH, Kim KS, Culley DE, Reed SB, Romine MF, Saffarini DA, Hill EA, Shi L, Elias DA, Kennedy DW, Pinchuk G, Watanabe K, Ishii S, Logan B, Nealson KH, Fredrickson JK. 2006. Electrically conductive bacterial nanowires produced by Shewanella oneidensis strain MR-1 and other microorganisms. Proc Natl Acad Sci U S A 103:11358–11363. https://doi.org/10.1073/pnas.0604517103.
41. Marsili E, Baron DB, Shikhare ID, Coursolle D, Gralnick JA, Bond DR. 2008. Shewanella secretes flavins that mediate extracellular electron transfer. Proc Natl Acad Sci U S A 105:3968–3973. https://doi.org/10.1073/pnas.0710525105.
42. Okamoto A, Nakamura R, Hashimoto K. 2011. In-vivo identification of direct electron transfer from Shewanella oneidensis MR-1 to electrodes via outer-membrane OmcA-MtrCAB protein complexes. Electrochim Acta 56:5526–5531. https://doi.org/10.1016/j.electacta.2011.03.076.
43. von Canstein H, Ogawa J, Shimizu S, Lloyd JR. 2008. Secretion of flavins by Shewanella species and their role in extracellular electron transfer. Appl Environ Microbiol 74:615–623. https://doi.org/10.1128/AEM.01387-07.
44. Reardon PN, Mueller KT. 2013. Structure of the type IVa major pilin from the electrically conductive bacterial nanowires of Geobacter sulfurreducens. J Biol Chem 288:29260–29266. https://doi.org/10.1074/jbc.M113.498527.
45. Reguera G, Pollina RB, Nicoll JS, Lovley DR. 2007. Possible nonconductive role of Geobacter sulfurreducens pilus nanowires in biofilm formation. J Bacteriol 189:2125–2127. https://doi.org/10.1128/JB.01284-06.
46. Smith JA, Tremblay PL, Shrestha PM, Snoeyenbos-West OL, Franks AE, Nevin KP, Lovley DR. 2014. Going wireless: Fe(III) oxide reduction without pili by Geobacter sulfurreducens strain JS-1. Appl Environ Microbiol 80:4331–4340. https://doi.org/10.1128/AEM.01122-14.
47. Wang VB, Chua SL, Cao B, Seviour T, Nesatyy VJ, Marsili E, Kjelleberg S, Givskov M, Tolker-Nielsen T, Song H, Loo JS, Yang L. 2013. Engineering PQS biosynthesis pathway for enhancement of bioelectricity production

Downloaded from mbio.asm.org on May 14, 2018 - Published by mbio.asm.org

in Pseudomonas aeruginosa microbial fuel cells. PLoS One 8:e63129. https://doi.org/10.1371/journal.pone.0063129.
48. Ramsey M, Hartke A, Huycke M. 2014. The physiology and metabolism of enterococci. *In* Gilmore MS, Clewell DB, Ike Y, Shankar N (ed), Enterococci: from commensals to leading causes of drug-resistant infection. Massachusetts Eye and Ear Infirmary, Boston, MA.
49. Abbaspour N, Hurrell R, Kelishadi R. 2014. Review on iron and its importance for human health. J Res Med Sci 19:164–174.
50. Giraffa G. 2002. Enterococci from foods. FEMS Microbiol Rev 26:163–171. https://doi.org/10.1111/j.1574-6976.2002.tb00608.x.
51. Byappanahalli M, Fujioka R. 2004. Indigenous soil bacteria and low moisture may limit but allow faecal bacteria to multiply and become a minor population in tropical soils. Water Sci Technol 50:27–32.
52. Junqueira ACM, Ratan A, Acerbi E, Drautz-Moses DI, Premkrishnan BNV, Costea PI, Linz B, Purbojati RW, Paulo DF, Gaultier NE, Subramanian P, Hasan NA, Colwell RR, Bork P, Azeredo-Espin AML, Bryant DA, Schuster SC. 2017. The microbiomes of blowflies and houseflies as bacterial transmission reservoirs. Sci Rep 7:16324. https://doi.org/10.1038/s41598-017-16353-x.
53. Lebreton F, Willems RJL, Gilmore MS. 2014. Enterococcus diversity, origins in nature, and gut colonization. *In* Gilmore MS, Clewell DB, Ike Y, Shankar N (ed), Enterococci: from commensals to leading causes of drug resistant infection. Massachusetts Eye and Ear Infirmary, Boston, MA.
54. Marsili E, Rollefson JB, Baron DB, Hozalski RM, Bond DR. 2008. Microbial biofilm voltammetry: direct electrochemical characterization of catalytic electrode-attached biofilms. Appl Environ Microbiol 74:7329–7337. https://doi.org/10.1128/AEM.00177-08.
55. Schröder U, Harnisch F, Angenent LT. 2015. Microbial electrochemistry and technology: terminology and classification. Energy Environ Sci 8:513–519. https://doi.org/10.1039/C4EE03359K.
56. Shi L, Richardson DJ, Wang Z, Kerisit SN, Rosso KM, Zachara JM, Fredrickson JK. 2009. The roles of outer membrane cytochromes of Shewanella and Geobacter in extracellular electron transfer. Environ Microbiol Rep 1:220–227. https://doi.org/10.1111/j.1758-2229.2009.00035.x.
57. Chen GY, McDougal CE, D'Antonio MA, Portman JL, Sauer J-D. 2017. A genetic screen reveals that synthesis of 1,4-dihydroxy-2-naphthoate (DHNA), but not full-length menaquinone, is required for Listeria monocytogenes cytosolic survival. mBio 8:e00119-17. https://doi.org/10.1128/mBio.00119-17.
58. Poole RK, Cook GM. 2000. Redundancy of aerobic respiratory chains in bacteria? Routes, reasons and regulation. Adv Microb Physiol 43:165–224. https://doi.org/10.1016/S0065-2911(00)43005-5.
59. Wrighton KC, Thrash JC, Melnyk RA, Bigi JP, Byrne-Bailey KG, Remis JP, Schichnes D, Auer M, Chang CJ, Coates JD. 2011. Evidence for direct electron transfer by a Gram-positive bacterium isolated from a microbial fuel cell. Appl Environ Microbiol 77:7633–7639. https://doi.org/10.1128/AEM.05365-11.
60. Liu M, Yuan Y, Zhang LX, Zhuang L, Zhou SG, Ni JR. 2010. Bioelectricity generation by a Gram-positive Corynebacterium sp. strain MFC03 under alkaline condition in microbial fuel cells. Bioresour Technol 101:1807–1811. https://doi.org/10.1016/j.biortech.2009.10.003.
61. Kim GT, Hyun MS, Chang IS, Kim HJ, Park HS, Kim BH, Kim SD, Wimpenny JW, Weightman AJ. 2005. Dissimilatory Fe(III) reduction by an electrochemically active lactic acid bacterium phylogenetically related to Enterococcus gallinarum isolated from submerged soil. J Appl Microbiol 99:978–987. https://doi.org/10.1111/j.1365-2672.2004.02514.x.
62. Lechardeur D, Cesselin B, Fernandez A, Lamberet G, Garrigues C, Pedersen M, Gaudu P, Gruss A. 2011. Using heme as an energy boost for lactic acid bacteria. Curr Opin Biotechnol 22:143–149. https://doi.org/10.1016/j.copbio.2010.12.001.
63. Richardson DJ. 2000. Bacterial respiration: a flexible process for a changing environment. Microbiology 146:551–571. https://doi.org/10.1099/00221287-146-3-551.
64. Baureder M, Hederstedt L. 2012. Genes important for catalase activity in Enterococcus faecalis. PLoS One 7:e36725. https://doi.org/10.1371/journal.pone.0036725.
65. Pedersen MB, Gaudu P, Lechardeur D, Petit MA, Gruss A. 2012. Aerobic respiration metabolism in lactic acid bacteria and uses in biotechnology. Annu Rev Food Sci Technol 3:37–58. https://doi.org/10.1146/annurev-food-022811-101255.
66. Rezaïki L, Lamberet G, Derré A, Gruss A, Gaudu P. 2008. Lactococcus lactis produces short-chain quinones that cross-feed group B Streptococcus to activate respiration growth. Mol Microbiol 67:947–957. https://doi.org/10.1111/j.1365-2958.2007.06083.x.
67. Miethke M, Marahiel MA. 2007. Siderophore-based iron acquisition and pathogen control. Microbiol Mol Biol Rev 71:413–451. https://doi.org/10.1128/MMBR.00012-07.
68. Waldron KJ, Robinson NJ. 2009. How do bacterial cells ensure that metalloproteins get the correct metal? Nat Rev Microbiol 7:25–35. https://doi.org/10.1038/nrmicro2057.
69. Dunny GM, Brown BL, Clewell DB. 1978. Induced cell aggregation and mating in Streptococcus faecalis: evidence for a bacterial sex pheromone. Proc Natl Acad Sci U S A 75:3479–3483. https://doi.org/10.1073/pnas.75.7.3479.
70. Debroy S, van der Hoeven R, Singh KV, Gao P, Harvey BR, Murray BE, Garsin DA. 2012. Development of a genomic site for gene integration and expression in Enterococcus faecalis. J Microbiol Methods 90:1–8. https://doi.org/10.1016/j.mimet.2012.04.011.
71. Rana NF, Sauvageot N, Laplace JM, Bao Y, Nes I, Rincé A, Posteraro B, Sanguinetti M, Hartke A. 2013. Redox balance via lactate dehydrogenase is important for multiple stress resistance and virulence in *Enterococcus faecalis*. Infect Immun 81:2662–2668. https://doi.org/10.1128/IAI.01299-12.
72. Paganelli FL, Willems RJ, Jansen P, Hendrickx A, Zhang X, Bonten MJ, Leavis HL. 2013. Enterococcus faecium biofilm formation: identification of major autolysin AtlAEfm, associated Acm surface localization, and AtlAEfm-independent extracellular DNA release. mBio 4:e00154-13. https://doi.org/10.1128/mBio.00154-13.
73. Schindelin J, Arganda-Carreras I, Frise E, Kaynig V, Longair M, Pietzsch T, Preibisch S, Rueden C, Saalfeld S, Schmid B, Tinevez JY, White DJ, Hartenstein V, Eliceiri K, Tomancak P, Cardona A. 2012. Fiji: an open-source platform for biological-image analysis. Nat Methods 9:676–682. https://doi.org/10.1038/nmeth.2019.
74. Sbalzarini IF, Koumoutsakos P. 2005. Feature point tracking and trajectory analysis for video imaging in cell biology. J Struct Biol 151:182–195. https://doi.org/10.1016/j.jsb.2005.06.002.
75. R Core Team. 2016. R: a language and environment for statistical computing.
76. Rolfe MD, Rice CJ, Lucchini S, Pin C, Thompson A, Cameron AD, Alston M, Stringer MF, Betts RP, Baranyi J, Peck MW, Hinton JC. 2012. Lag phase is a distinct growth phase that prepares bacteria for exponential growth and involves transient metal accumulation. J Bacteriol 194:686–701. https://doi.org/10.1128/JB.06112-11.

Downloaded from mbio.asm.org on May 14, 2018 - Published by mbio.asm.org